Slip pulse and resonance of Kathmandu basin during the 2015 Gorkha earthquake, Nepal

Authors: John Galetzka[1+], Diego Melgar[2], Joachim F. Genrich[1], Jianghui Geng[3], Susan Owen[4], Eric O. Lindsey[3], Xiaohua Xu[3], Yehuda Bock[3], Jean-Philippe Avouac[5,1*], Lok Bijaya Adhikari [6], Bishal Nath Upreti[7], Beth Pratt-Sitaula[8], Tara Nidhi Bhattarai[9], Bhairab P Sitaula[9,], Angelyn Moore[4], Kenneth W. Hudnut[10], Walter Szeliga[11], Jim Normandeau[12], Michael Fend[12], Mireille Flouzat[13], Laurent Bollinger[13], Prithvilal Shrestha[6], Bharat Koirala[6], Umesh Gautam[6], Mukunda Bhatterai[6], Ratnamani Gupta[6], Thakur Kandel[6], Chintan Timsina[6], Soma Nath Sapkota[6], Sudhir Rajaure[6], Naresh Maharjan[6]

Affiliations:
[1] California Institute of Technology, Department of Geology and Planetary Sciences, Pasadena, CA, USA.
[2]University of California Berkeley, Seismological Laboratory, Berkeley, CA, USA.
[3]Cecil H. and Ida M. Green Institute of Geophysics and Planetary Physics, Scripps Institution of Oceanography, University of California San Diego, La Jolla, CA, USA.
[4]Jet Propulsion Laboratory, California Institute of Technology, Pasadena, CA 91109, USA.
[5]University of Cambridge, Department of Earth Sciences, Cambridge, UK.
[6]Department of Mines and Geology, Kathmandu, Nepal.
[7]Nepal Academy of Science and Technology (NAST) Khumaltar, Lalitpur, Nepal
[8] Geological Sciences Department, Central Washington University
[9]Tri-Chandra Campus, Tribhuvan University, Ghantaghar, Kathmandu Nepal
[10] US Geological Survey, Pasadena, CA, USA.
[11]PAcific Northwest Geodetic Array and Geological Sciences, Central Washington University
[12]UNAVCO Inc., Boulder, CO, USA
[13] CEA, DAM, DIF, Arpajon, France, France.
[+] Now at UNAVCO Inc., Boulder, CO, USA.
*Correspondence to: avouac@gps.caltech.edu

Detailed geodetic imaging of earthquake rupture enhances our understanding of earthquake physics and induced ground shaking. The April 25, 2015 Mw 7.8 Gorkha, Nepal earthquake is the first example of a large continental megathrust rupture beneath a high-rate (5 Hz) GPS network. We use GPS and InSAR data to model the earthquake rupture as a slip pulse of ~20 km width, ~6 s duration, and with peak sliding velocity of 1.1 m/s that propagated toward Kathmandu basin at ~3.3 km/s over ~140 km. The smooth slip onset, indicating a large ~5 m slip-weakening distance, caused moderate ground shaking at high >1Hz frequencies (~16% g) and limited damage to regular dwellings. Whole basin resonance at 4-5 s period caused collapse of tall structures, including cultural artifacts.

One sentence summary: High-rate GPS records reveal that the Gorkha earthquake resulted from eastward propagation of a ~6s long slip pulse, with smooth onset which generated mild ground shaking but exited resonance of Kathmandu basin at ~4-5 s.

The shape of the slip-rate time function (STF) during seismic rupture provides critical insight into constitutive fault properties. The abruptness of slip onset determines the high frequency content and hence the intensity of the near-field ground motion (*1*), whereas the tail, which discriminates pulse-like and crack-like ruptures (*2*), has a low frequency signature. Therefore, resolving the STF with band-limited strong motion records is difficult. The combination of high-rate GPS waveforms (*3, 4*), which capture both dynamic and permanent deformation, overcomes this limitation.

The April 25th 2015 M_w 7.8 Gorkha, Nepal earthquake resulted from unzipping of the lower edge of the locked portion of the Main Himalayan Thrust (MHT) thrust fault, along which the Himalayan wedge is thrust over India (*5*). The earthquake nucleated ~80 km northwest of Kathmandu and ruptured a 140 km long segment of the fault (Figure 1A) with a hypocentral depth of ~15 km and a dip angle of 7-12°(*5, 6*). The MHT accommodates the majority of the convergence between India and southern Tibet with a rate between 17 and 21 mm/yr (*7*). For the 2015 event, which resulted in over 8,000 deaths, mostly in the Kathmandu and adjacent districts, Mercali shaking intensities (MMI) reported by the National Society for Earthquake Technology (*8*) reached up to IX (violent) and exceeded VI (strong) over a 170x40 km^2 area. Kathmandu has been struck by repeated earthquakes in the past, with major destruction (MMI>X, extreme) in 1255, 1344, 1408, 1681, 1833 and 1934 (*9-11*). These earthquakes all occurred close to Kathmandu and have been assigned magnitudes between Mw 7.5 and 8.4. Damages in the Kathmandu basin were probably amplified by site effects during the Gorkha earthquake as happened with past events (*12, 13*). The basin is filled with 500-600 m of fluviolacustrine sediments resting on metamorphic basement (*14*).

The damage to the most vulnerable vernacular dwellings in Kathmandu, which rarely exceed 4 stories, was in fact much less than expected in view of the 2015 earthquake's magnitude and its proximity to Kathmandu. By contrast, some taller structures were more severely affected, such as the 60 m tall Dharahara tower which collapsed, but had partially survived the Mw 8.1-8.4 1934 earthquake.. The 1934 event induced much more extensive destruction to vernacular dwellings in Kathmandu than in 2015 (20% of the buildings in Kathmandu were destroyed in 1934, less than 1% in 2015) *(15)*. These observations reflect the combined effects of the source characteristics and local geological conditions, in addition to evolution of building practices.

The 2015 Gorkha earthquake ruptured a subhorizontal portion of the MHT lying directly beneath a network *(16)* of continuous GPS (cGPS) stations recording at a high rate of 5 samples per second, and one accelerometer station *(17)* (Fig. 1A). In addition, surface displacements were measured with interferometric synthetic aperture radar, InSAR,(*18, 19*) (fig. S1). While a number of recent earthquakes were documented with similar techniques *(20, 21)*, the Gorkha event is the first occurrence of a large continental thrust earthquake to be observed by high-rate cGPS stations at very close distances to and completely encompassing the rupture area. The combination of these measurements provide the opportunity to image the kinematics of the source process and the strong ground motion that led to the particular pattern of structural damage observed during this earthquake.

The records of seismic displacements and accelerations (Figs. 2 and S2) show southward motion of up to 2 m, with a rise time on the order of 6 seconds. The pulse is particularly clear at cGPS station KKN4 located on bedrock just north of Kathmandu and

only ~13 km above the fault. The displacement at this station started at about 25 s after the onset of rupture, corresponding to 15 seconds after P-waves arrival time (Fig.2), and reached its final static value by about 32 s, using the USGS origin time of radiated direct P waves at 06:11:26.270 UTC *(6)*. The records clearly indicate a pulse-like rupture (*22*) with slip on any given portion of the fault occurring over a short fraction of the total ~70 s duration of the earthquake source *(5)*. Given the ~78 km distance of KKN4 to the epicenter, the pulse must have propagated at ~3 km/s, a value consistent with waveform modeling and back projection of high frequency seismic waves recorded at teleseismic distances *(5)*. Surface velocities reached values of ~0.7 m/s. The cGPS station NAST within Kathmandu basin shows, in addition to the pulse seen at KKN4, strong oscillations of period of about 3-4 seconds lasting for ~20 s (Figs. 2 and 3A). The Gorkha earthquake must have excited a resonance of the Kathmandu basin as a whole. The resonance is clearly shown in the response spectra from these stations as well as from the accelerometer station KATNP (Fig 3G-I).

To retrieve the kinematics of the seismic rupture, we carried out a formal inversion of time-dependent slip on the fault *(23, 24)* and compared the recorded waveforms with forward predictions assuming a propagating slip pulse with varied characteristics. We assumed a planar fault geometry with a strike of 295° and a dip of 11° in accordance with the teleseismic W-phase moment tensor solution from the USGS (*6*). We tested shallower dips up to 7° but found that 11° provided a better fit to the data. The fault was discretized into 10x10 km subfault segments. We jointly inverted the three-component, 5 Hz GPS derived velocity waveforms, the GPS static offsets, and the InSAR line of sight (LOS) static displacements measured between February 22 and May 3 (fig. S1). The GPS displacement time series shows large postseismic motion at only one station (CHLM) with less than 2 cm magnitude on both the horizontal and vertical over the week following the earthquake. Therefore, for our purposes, we neglect the contribution of postseismic deformation to the LOS displacements.. The model fits both data sets closely (Figs. 1A), with 86% variance reduction for the InSAR and GPS coseismic displacements and 74% variance reduction for the GPS velocity waveforms (Figs. S2, S4). The model indicates predominantly unilateral rupture to the southeast with peak slip of ~6.5 m on a large asperity to the north of Kathmandu. The event duration is 65 s (fig. S4) with peak moment release at 23 s when the slip pulse is less than 10 km north of Kathmandu (movie S1), and peak slip-rate is 1.1 m/s. Most of the slip is concentrated within a narrow region between the 10 and 20 km fault depth contours. We find a large asperity with 3.0 m of slip due east of the main asperity and between 20 and 23 km depth. The rupture velocity of the propagating slip pulse indicated by the onset of slip in our best-fitting model is ~3.2 km/s and has a maximum allowed velocity of 3.3 km/s (fig. S4). This velocity corresponds to ~95% of the shear wave speed at the depth of the majority of slip (15 km) according to the local velocity model used to calculate the Green's functions (Table S2), indicating a very fast rupture propagation. Slip tapers at 17-20 km depth along the edge of the locked zone of the MHT. The inversion has a large number of parameters, which allows for a relatively complex rupture history. However, the resulting model is remarkably simple with essentially a single propagating slip pulse. The spatio-temporal evolution of the slip pulse matches well the location of the sources of high frequency (0.5-2Hz) seismic waves derived from the back projection of the teleseismic waveforms (*5*) (Movie S1).

We calculated the static stress change on the fault plane due to the earthquake (Fig. 1B). It shows loading of the fault around the main asperity where most of the aftershocks occurred, including the Mw 7.3 aftershock of May 12, as expected from triggering by coseismic stress transfer *(25)*. The model predicts a pattern of uplift of the Kathmandu basin and subsidence at the front of the high range (fig. S4), approximately opposite to the pattern observed in the interseismic period as expected from simple models of the seismic cycle on the MHT (*26, 27*).

The record at station KKN4 should be a close representation of the slip-rate time function as it lies only about 13 km above the propagating slip pulse and is not affected by the site effects seen at the stations in Kathmandu basin. We conducted synthetic tests with the same Earth structure model used in the inversion (Table S1) to assess the distortion and smoothing introduced by the elastic half space response (fig. S5). We found a vertical velocity amplitude of about 70% of the peak slip rate on the fault directly beneath it along with a well-preserved temporal shape. Furthermore, the tests demonstrate that the smooth onset of slip is not an artifact resulting from the transfer through the elastic medium represented by the elastodynamic Green's functions. The shape of the slip pulse can also be retrieved from the GPS records at NAST and strong motion vertical records at KATNP which are less affected by site effects than the horizontal records (Fig. 1). All three records indicate a ~6 s duration pulse. The shape of the pulse fits the regularized Yoffe function *(28)* yielding a rather smooth rise, with an acceleration time to peak slip rate of τ_s=1.7 s, a rise time of τ_R=3.3 s and a total effective duration of τ_{eff} =6.7 s. The slip-rate pulse derived from the inversion is also well fit using the same values of τ_s and τ_R s and peak slip-rate of ~0.9 m/s (Fig. 4). We compared the recorded waveforms with predictions from a suite of forward models to test the robustness of our results. We used the static slip model in these tests deduced from the inversion of the GPS static and InSAR measurements (Fig. S7). We assumed a propagating slip pulse with varying characteristics using the regularized Yoffe STF. We varied the rupture velocity between 2.8 and 3.6 km/s, and the rise time between 2 and 10s (fig. S8). We also tested the resolution power of the inversion and the limited bias introduced by the regularization applied to the inversions by inverting synthetics calculated from forward modeling (24, fig. S10, fig. S11).Together, these tests demonstrate the duration of the slip pulse is probably less than 10 s and the time to the peak-slip rate cannot be shorter than 1 s (we would otherwise observe a much larger amplitude at high frequencies) and the average propagation rate of the slip pulse is not less than ~3.0 km/s over the first 30 s (until KKN4, NAST and KATNP records a pulse signal).

Tinti et al *(28)* analyzed how the shape of the STF relate to the characteristics of the friction law governing the dynamics of the rupture. Based on this rationale (their equations 6 and 11), we estimate the slip-weakening distance to be ~5 m (for a peak-slip of 6.5 m). The distance is a large value compared to those estimated from kinematic and dynamic modeling of seismic ruptures (*29, 30*), which tend to be overestimated *(1)* and are typically on the order of 0.5 to 1 m. The large value we obtained is possibly related to the earthquake occurring close to the brittle-ductile transition at the lower edge of the locked portion of the MHT. The modeled smooth onset of the STF and the related large slip-weakening distance provide an explanation of the relatively low amplitude of shaking at frequencies above 1 Hz. The observed slip-weakening behavior does not require the friction law to be actually slip-weakening. A fault obeying rate and state friction can show an effective slip-

weakening behavior with an effective critical distance several orders of magnitude larger that the critical distance entering the friction law *(31)*. Aspects of the rupture kinematics and ground strong motion observed during the Gorkha event may also be due to hanging wall effects, the importance of which could be assessed through dynamic modeling of the rupture (*32, 33*).

Our study provides insight into the main factors that determined damage sustained during the Gorkha earthquake. While the hypocenter was ~80 km away from the city, the main asperity that radiated most of the energy was much closer, just north of the basin and at relatively shallow depth. Comparison of the waveforms recorded within the sedimentary basin at NAST and KATNP (fig. 3) with the bedrock records at KKN4 shows prominent differences even though the stations are less than 13 km apart. The waveforms at the bedrock station KKN4 are simple, mostly dominated by the single pulse, while within the basin peak horizontal ground velocities of 0.5 to 0.8 m/s (considered severe to violent, *(34)*) are sustained for 20 s at KATNP and 40 s at NAST. The ratio of the amplitude spectra of the basin waveforms to those at the hill station (Fig. 2D-F) shows amplification of long period energy between 1 and 9 s with the basin amplitudes being 6-7 times larger in the horizontal direction than at the bedrock station. The response spectra (Fig. 2G-I) show that, within this amplified period band, it was the 4 s period shaking that was the strongest at the basin stations.

The 4 s peak in the response spectra coincides with the observation that the source time function beneath Kathmandu likely had a duration of ~6-7 s. The net effect of this long source duration with slow onset time is to produce radiation that is depleted of high frequency energy (fig. S11). This explains why vernacular dwellings with only a few stories were not severely affected despite the anticipated short period site effects from microzoning *(13)*. Furthermore, high frequency intensity measurements such as peak ground accelerations were modest (Fig 2, ~1.6 m/s^2, MMI VI), while longer period intensity measures such as peak ground velocity (Fig 3) were very large (80 cm/s, MMI IX). Kathmandu was faced with a combination of source and site effects. Rupture directivity focused radiated seismic energy towards the city; the smooth onset and 6-7 second duration of the pulse excited a resonance of the Kathmandu basin, producing protracted duration of violent shaking at a period around 4s.

Acknowledgments

The GPS data are available from the UNAVCO website. The INSAR data are available at http://topex.ucsd.edu/nepal/. The Nepal Geodetic Array was funded by internal funding to JPA from Caltech and DASE and by the Gordon and Betty Moore Foundation, through Grant GBMF 423.01 to the Caltech Tectonics Observatory and was maintained thanks to NSF Grant EAR 13-45136. Andrew Miner and the PAcific Northwest Geodetic Array (PANGA) at Central Washington University are thanked for technical assistance with the construction and operation of the Tribhuvan University-CWU network. Additional funding for the TU-CWU network came from United Nations Development Programme and Nepal Academy for Science and Technology. The high rate data were recovered thanks to a rapid intervention funded by NASA (US) and the Department of Foreign International Development (UK). We thank Trimble Navigation Ltd and the Vaidya family for supporting the rapid response as well. The accelerometer record at KATNP was provided by USGS. Research at UC Berkeley was funded by the Gordon and Betty Moore Foundation through grant GBMF 3024. A

portion of this work was carried out at the Jet Propulsion Laboratory, California Institute of Technology, under a contract with the National Aeronautics and Space Administration. The GPS data were processed by ARIA (JPL) and the Scripps Orbit and Permanent Array Center. The effort at the Scripps Institution of Oceanography was funded by NASA grants NNX14AQ53G and NNX14AT33G. ALOS-2 data were provided under JAXA (Japan) PI Investigations 1148 and 1413. JPA thanks the Royal Society for support. We thank Susan Hough, Doug Given, Irving Flores and Jim Luetgert for contribution to the installation of this station. We thank Doug Dreger for discussion and Walter Mooney for comments.

Authors contributions: Jean-Philippe Avouac led the study and wrote the article. Diego Melgar did the kinematic modeling and wrote the article. Yehuda Bock supervised the high-rate data processing and wrote the article. John Galetzka led the field operations. Jianghui Geng conducted the high rate data processing. Sue Owen, Angelyn Moore, Walter Szeliga and Jeff Genrich conducted the low rate data analysis to estimate co-seismic offsets. Eric Lindsey and Xiaohua Xu conducted the InSAR data processing. Lok Bijaya helped organizing the field operations. All other authors contributed to building and servicing the GPS stations and to the post-earthquake data recovery. All authors edited the article.

References and Notes

References

1. M. Guatteri, P. Spudich, What can strong-motion data tell us about slip-weakening fault- friction laws? *Bulletin of the Seismological Society of America* **90**, 98-116 (2000).
2. X. Lu, N. Lapusta, A. J. Rosakis, Pulse-like and crack-like ruptures in experiments mimicking crustal earthquakes. *Proceedings of the National Academy of Sciences of the United States of America* **104**, 18931-18936 (2007).
3. R. M. Nikolaidis, Y. Bock, P. J. de Jonge, P. Shearer, D. C. Agnew, M. Van Domselaar, Seismic wave observations with the Global Positioning System. *Journal of Geophysical Research-Solid Earth* **106**, 21897-21916 (2001); (10.1029/2001jb000329).
4. G. L. Emore, J. S. Haase, K. Choi, K. A. Larson, A. Yamagiwa, Recovering seismic displacements through combined use of 1-Hz GPS and strong-motion accelerometers. *Bulletin of the Seismological Society of America* **97**, 357-378 (2007).
5. J.-P. Avouac, L. Meng, S. Wei, W. Wang, J.-P. Ampuero, Lower edge of locked Main Himalayan Thrust unzipped by the 2015 Gorkha earthquake. *Nature Geoscience*, (submitted); (10.1038/ngeo2518).
6. USGS, http://earthquake.usgs.gov/earthquakes/eventpage/us20002ejl - general_summary.
7. T. Ader, J. P. Avouac, J. Liu-Zeng, H. Lyon-Caen, L. Bollinger, J. Galetzka, J. Genrich, M. Thomas, K. Chanard, S. N. Sapkota, S. Rajaure, P. Shrestha, L. Ding, M. Flouzat, Convergence rate across the Nepal Himalaya and interseismic coupling on the Main Himalayan Thrust: Implications for seismic hazard. *Journal of Geophysical Research-Solid Earth* **117**, (2012); (10.1029/2011jb009071).

8. NSET, Intensity maps of the Mw7.8 Gorkha earthquake, National Society for Earthquake Technology-Nepal, http://www.nset.org.np/eq2015/intensity_maps.php. (2015).
9. J. L. Mugnier, P. Huyghe, A. P. Gajurel, B. N. Upreti, F. Jouanne, Seismites in the Kathmandu basin and seismic hazard in central Himalaya. *Tectonophysics* **509**, 33-49 (2011); (10.1016/j.tecto.2011.05.012).
10. R. Bilham, Location and Magnitude of the 1833 Nepal Earthquake and Its Relation to the Rupture Zones of Contiguous Great Himalayan Earthquakes. *Current Science* **69**, 101-128 (1995).
11. M. R. Pant, in *Adarsa*. (Odisha, India, 2002), vol. 2, pp. 29-60.
12. A. Dixit, Dwelly-Samant, L., Nakarmi,M., Tucker, B., Pradhanang, S., The Kathmandu valley Earthquake management plan. Published by National Society for Earthquake Technology-Nepal37 pp. http://www.preventionweb.net/english/professional/publications/. (1998).
13. Y. R. Paudyal, R. Yatabe, N. P. Bhandary, R. K. Dahal, A study of local amplification effect of soil layers on ground motion in the Kathmandu Valley using microtremor analysis. *Earthquake Engineering and Engineering Vibration* **11**, 257-268 (2012); (10.1007/s11803-012-0115-3).
14. S. Moribayashi, Y. Maruo, Basement topography of the Kathmandu valley Nepal: an application of gravitational method to the survey of a tectonic basin in Himalayas. *J. Jap. Soc. Eng. Geol.* **21**, 30-37 (1980).
15. B. S. J. B. Rana, *Nepalako mahabhukampa (1990 sala) Nepal's great earthquake*. B. S. J. B. Rana, Ed., (1935).
16. The Nepal Geodetic Array (http://www.tectonics.caltech.edu/resources/kmlnepal.html) was deployed as a result of a collaboration between the Caltech Tectonics Observatory (US), the Department of Mines and Geology of (Nepal) and the Department Analyse et Surveillance de l'Environnement (CEA, France).
17. USGS, Earthquake Hazards Program- NetQuakes: Station KATNP_NQ_01, http://earthquake.usgs.gov/monitoring/netquakes/station/KATNP_NQ_01/20150425061138/.
18. E. Lindsey, R. Natsuaki, X. Xu, M. Shimada, H. Hashimoto, and D. Sandwell,, Gorkha Mw 7.8 Earthquake: Line of Sight Deformation from ALOS-2 Interferometry, http://topex.ucsd.edu/nepal. *Seismological Research Letters*, (in prep).
19. ESA, Nepal earthquake: Sentinel-1 InSAR analyis, April 2015, http://insarap.org/.
20. C. Ji, K. M. Larson, Y. Tan, K. W. Hudnut, K. H. Choi, Slip history of the 2003 San Simeon earthquake constrained by combining 1-Hz GPS, strong motion, and teleseismic data. *Geophysical Research Letters* **31**, (2004); (10.1029/2004gl020448).
21. H. Yue, T. Lay, S. Y. Schwartz, L. Rivera, M. Protti, T. H. Dixon, S. Owen, A. V. Newman, The 5 September 2012 Nicoya, Costa Rica M-w 7.6 earthquake rupture process from joint inversion of high-rate GPS, strong-motion, and teleseismic P wave data and its relationship to adjacent plate boundary interface properties. *Journal of Geophysical Research-Solid Earth* **118**, 5453-5466 (2013); (10.1002/jgrb.50379).
22. T. H. Heaton, Evidence for and implications of self-healing pulses of slip in earthquake rupture. *Physics of the Earth and Planetary Interiors* **64**, 1-20 (1990).

23. D. Melgar, Y. Bock., Kinematic Earthquake Source Inversion and Tsunami Runup Prediction with Regional Geophysical Data. *Journal of Geophysical Research: Solid Earth* **120**, (2015); (10.1002/2014JB011832).
24. Materials and methods are available as supplementary material on Science Online.
25. R. S. Stein, The role of stress transfer in earthquake occurrence. *Nature* **402**, 605-609 (1999).
26. R. Bilham, K. Larson, J. Freymueller, F. Jouanne, P. LeFort, P. Leturmy, J. L. Mugnier, J. F. Gamond, J. P. Glot, J. Martinod, N. L. Chaudury, G. R. Chitrakar, U. P. Gautam, B. P. Koirala, M. R. Pandey, R. Ranabhat, S. N. Sapkota, P. L. Shrestha, M. C. Thakuri, U. R. Timilsina, D. R. Tiwari, G. Vidal, C. Vigny, A. Galy, B. deVoogd, GPS measurements of present-day convergence across the Nepal Himalaya. *Nature* **386**, 61-64 (1997).
27. R. Cattin, J. P. Avouac, Modeling mountain building and the seismic cycle in the Himalaya of Nepal. *Journal of Geophysical Research-Solid Earth* **105**, 13389-13407 (2000).
28. E. Tinti, E. Fukuyama, A. Piatanesi, M. Cocco, A kinematic source-time function compatible with earthquake dynamics. *Bulletin of the Seismological Society of America* **95**, 1211-1223 (2005); (10.1785/0120040177).
29. S. Ide, M. Takeo, Determination of constitutive relations of fault slip based on seismic wave analysis. *Journal of Geophysical Research-Solid Earth* **102**, 27379-27391 (1997).
30. T. Mikumo, K. B. Olsen, E. Fukuyama, Y. Yagi, Stress-breakdown time and slip-weakening distance inferred from slip-velocity functions on earthquake faults. *Bulletin of the Seismological Society of America* **93**, 264-282 (2003).
31. A. Bizzarri, M. Cocco, Slip-weakening behavior during the propagation of dynamic ruptures obeying rate- and state-dependent friction laws. *Journal of Geophysical Research-Solid Earth* **108**, (2003); (10.1029/2002jb002198).
32. J. E. Kozdon, E. M. Dunham, Rupture to the Trench: Dynamic Rupture Simulations of the 11 March 2011 Tohoku Earthquake. *Bulletin of the Seismological Society of America* **103**, 1275-1289 (2013); (10.1785/0120120136).
33. D. D. Oglesby, R. J. Archuleta, S. B. Nielsen, Earthquakes on dipping faults: The effects of broken symmetry. *Science* **280**, 1055-1059 (1998).
34. C. B. Worden, M. C. Gerstenberger, D. A. Rhoades, D. J. Wald, Probabilistic Relationships between Ground-Motion Parameters and Modified Mercalli Intensity in California. *Bulletin of the Seismological Society of America* **102**, 204-221 (2012); (10.1785/0120110156).

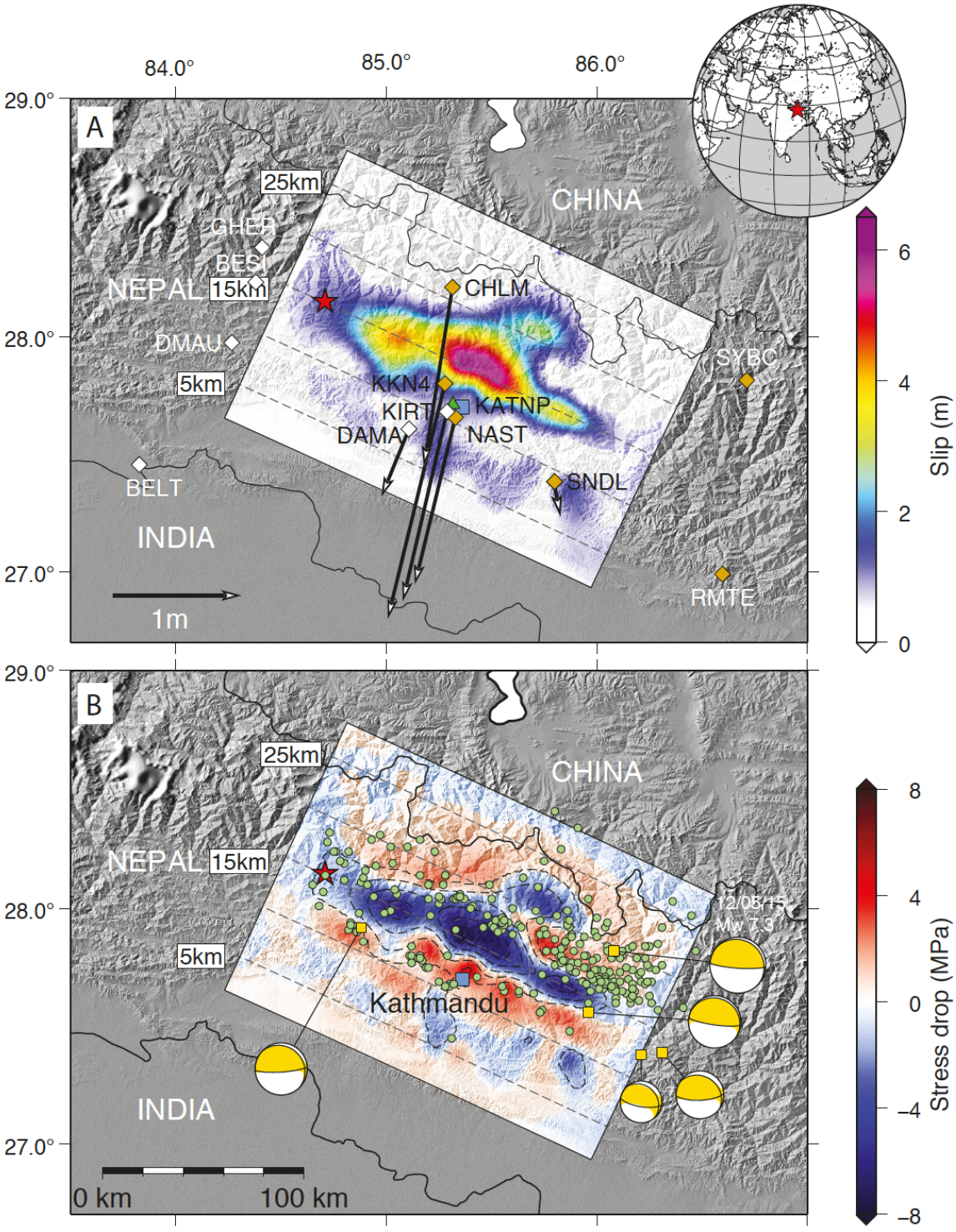

Figure 1: Cumulative slip distribution and static stress drop due to the Gorkha earthquake. (A) Slip inversion results for the Mw7.8 Gorkha event. The red star is the hypocenter. Dashed contours are depths to the fault. Orange diamonds are 5 Hz cGPS stations and white diamonds are low rate (1/30 Hz) stations. The green triangle is the strong motion station. Kathmandu is represented by the blue square. The black arrows

indicate the coseismic offsets measured at the sites (the values and uncertainties are given in Table S1). Vectors with less than 10cm displacement are not shown (B) Static stress drop predicted by the model of figure 1A. Green circles are aftershocks with local magnitude >4 recorded and located by the Nepal National Seismic Center. Focal mechanisms represent the GCMT moment tensors for aftershocks with magnitude larger than 6.

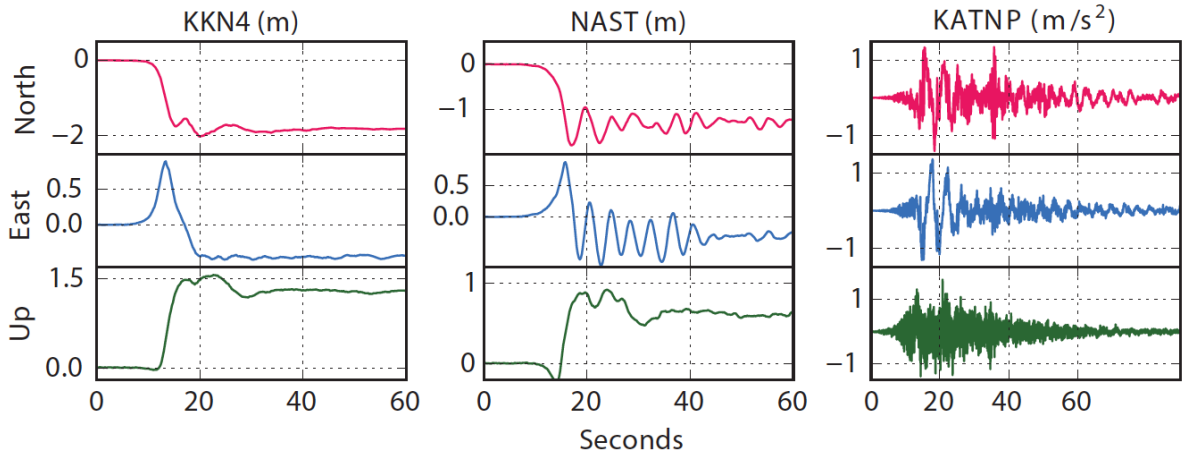

Figure 2: Records of ground displacements and accelerations during the Gorkha earthquake. Displacement waveforms at cGPS stations KKN4 and NAST (5 samples per second) and acceleration waveforms at strong motion station KATNP (figure 1).

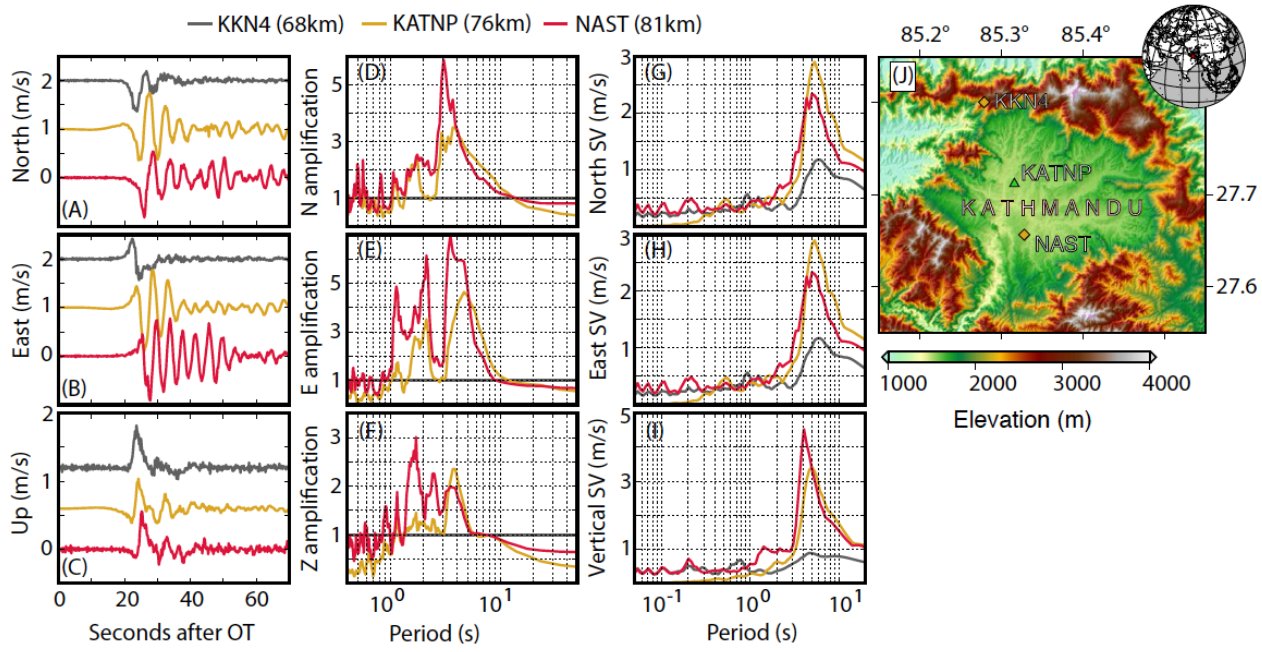

Figure 3: **Evidence for resonance of Kathmandu basin.** (A)-(C) three components of ground velocity observed at two high-rate GPS stations (KKN4 and NAST) and one strong motion station (KATNP) in the Kathmandu region. KKN4 is located on hard rock northwest

of Kathmandu while the other 2 stations are on soft sediment in the basin. The GPS is differentiated to velocity and the strong motion integrated after high-pass filtering at 0.02 Hz. (D)-(F) Ground motion amplification observed at the two basin stations. Plotted is the ratio of the amplitude spectra of the basin stations to the amplitude spectra of the reference bedrock station KKN4. (G)-(I) 5% damped velocity response spectra for all 3 stations. (J) Close up map showing the location of the basin and bedrock stations.

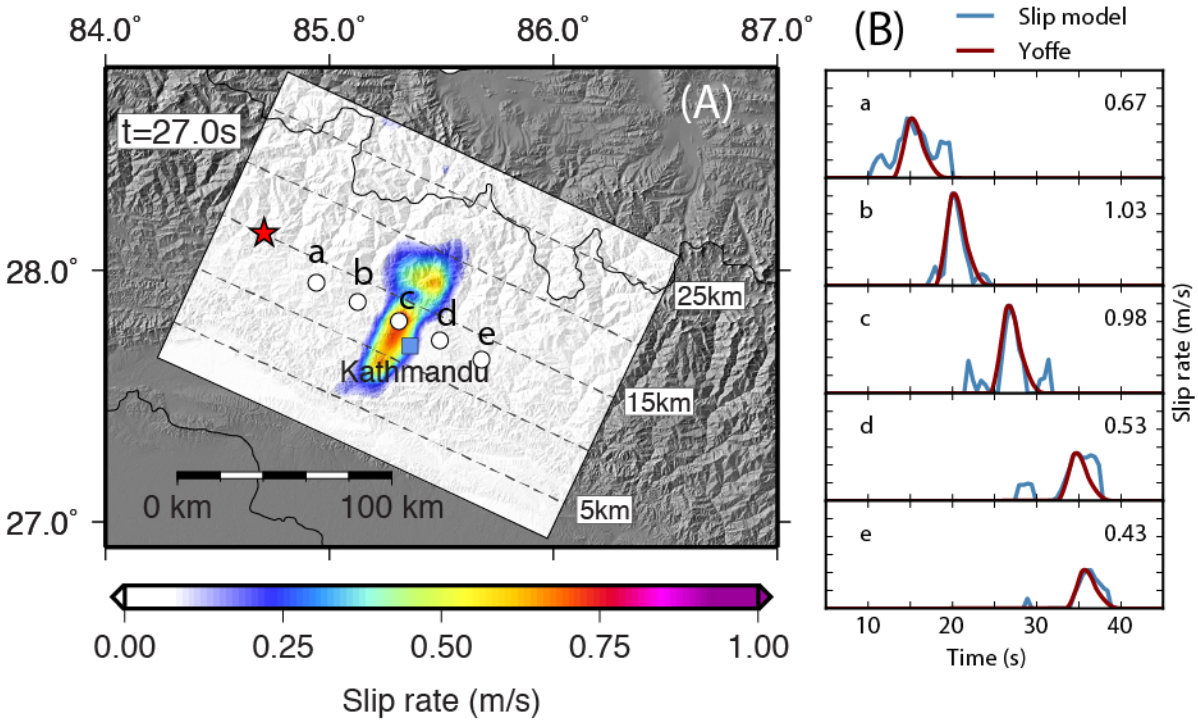

Figure 4: **Slip pulse kinematics during the Gorkha earthquake** (A) Snapshot of slip rate on Main Himalayan Thrust at 27 s after origin time during propagation of the seismic rupture from the model in figure 1. The red star is the hypocenter and dashed lines represent the depth to the fault. The white circles are the centers of 5 subfaults used to compare against theoretical regularized Yoffe source time functions(*28*). (B) STFs at the 5 locations from (A). Plotted are the inverted slip rates and the regularized Yoffe functions measured from the vertical velocity at KKN4 scaled to the maximum observed slip rate at each point which is indicated numerically. Time is relative to the hypocentral origin (28.147°N 84.708°E; 2015-04-25 06:11:26.270 UTC).

Supplementary Materials:

Materials and Methods

Figs. S1 to S11

Tab. S1 to S2

Movie S1

References (35–45)